J Solid State Electrochem (2011) 15:2633–2638
DOI 10.1007/s10008-010-1255-x

ORIGINAL PAPER

Effects of Cr doping on the electrochemical performance of $Li_3V_2(PO_4)_3$ cathode material for lithium ion batteries

S. Y. Yang · S. Zhang · B. L. Fu · Q. Wu · F. L. Liu · C. Deng

Received: 20 September 2010 / Revised: 12 November 2010 / Accepted: 15 November 2010 / Published online: 1 December 2010

Abstract A series of Cr-doped $Li_3V_{2-x}Cr_x(PO_4)_3$ (x=0, 0.1, 0.25, and 0.5) samples are prepared by a sol–gel method. The effects of Cr doping on the physical and chemical characteristics of $Li_3V_2(PO_4)_3$ are investigated. Compared with the XRD pattern of the undoped sample, the XRD patterns of the Cr-doped samples have no extra reflections, which indicates that Cr enters the structure of $Li_3V_2(PO_4)_3$. As indicated by the charge–discharge measurements, the Cr-doped $Li_3V_{2-x}Cr_x(PO_4)_3$ (x= 0.1, 0.25, and 0.5) samples exhibit lower initial capacities than the undoped sample at the 0.2 C rate. However, both the discharge capacity and cycling performance at high rates (e.g., 1 and 2 C) are enhanced with proper amount of Cr doping (x=0.1). The highest discharge capacity and capacity retention at the rates of 1 and 2 C are obtained for $Li_3V_{1.9}Cr_{0.1}(PO_4)_3$. The improvement of the electrochemical performance can be attributed to the higher crystal stability and smaller particle size induced by Cr doping.

Keywords Lithium vanadium phosphate · Cr doping · Sol–gel · Lithium ion battery

S. Y. Yang · S. Zhang (✉) · B. L. Fu · Q. Wu · F. L. Liu
College of Material Science and Chemical Engineering, Harbin Engineering University,
Harbin 150001, Heilongjiang, China
e-mail: senzhang@hrbeu.edu.cn

C. Deng (✉)
College of Chemistry and Chemical Engineering, Provincial Key Lab for Nano-functionalized Materials and Excitated States,
Harbin Normal University,
Harbin 150025, Heilongjiang, China
e-mail: chaodeng2008@yahoo.cn

Introduction

The need for large-scale batteries impels the development of new materials for lithium ion batteries. Recently, lithium transition metal phosphates such as $LiFePO_4$, $LiMnPO_4$ and $Li_3V_2(PO_4)_3$ have been extensively studied. In comparison with the conventional lithium transition metal oxides (e.g., $LiCoO_2$) cathode material, the phosphate-based materials exhibit many advantages such as low cost, nontoxicity, better thermal stability, etc. [1–3]. Among the phosphate-based materials, lithium vanadium phosphate has attracted considerable interests. $Li_3V_2(PO_4)_3$ can reversibly extract and insert two lithium ions based on the V^{3+}/V^{4+} redox. All the three lithium ions can be completely extracted and inserted when $Li_3V_2(PO_4)_3$ is cycled between 3.0 and 4.8 V, which results in a theoretical capacity of 197 mAh g^{-1}. Therefore, $Li_3V_2(PO_4)_3$ has been proposed as a highly promising cathode material for lithium ion batteries [4–6].

However, it is well known that the low electronic and ion conductivity of $Li_3V_2(PO_4)_3$ affect its electrochemical properties greatly. The improvements on the electronic or lithium ion conductivity can be achieved in three ways: metal ion doping [7, 8], particle size reducing [9, 10], and carbon coating [11, 12]. Individually and in combination, these methods have been used to improve the electrochemical performance of $Li_3V_2(PO_4)_3$. Many cations have been used to dope $Li_3V_2(PO_4)_3$, and some positive impacts are reported on its electrochemical performance [7, 8, 13, 14]. Baker et al. reports the Al^{3+} doping at V site in $Li_3V_2(PO_4)_3$. $Li_3V_{2-x}Al_x(PO_4)_3$ exhibits high material utilization and comparatively low discharge-capacity fade [13]. Ren et al. synthesize the $Li_3Fe_xV_{2-x}(PO_4)_3$ system,

and the improved electrochemical performance is obtained when x is 0.02–0.04 [14].

In this study, we investigated the impacts of Cr doping on the physical and electrochemical characteristics of $Li_3V_2(PO_4)_3$. The $Li_3V_{2-x}Cr_x(PO_4)_3$ (x=0, 0.1, 0.25, and 0.5) samples were prepared by a sol–gel method, and they were characterized and compared in detail.

Experimental

Synthesis of $Li_3V_{2-x}Cr_x(PO_4)_3$ (x = 0, 0.1, 0.25, and 0.5)

The samples were prepared by a sol–gel method. Stoichiometric amount of analytical reagents, $LiOH{\cdot}H_2O$, NH_4VO_3, $NH_4H_2PO_4$, $Cr(NO_3)_3$, and citric acid were used as the starting materials. All the reagents were first dissolved in the distilled water. Then the solution was kept at 80 °C under magnetic stirring. After a blue homogeneous solution is formed, the sol was taken out and dried at 80 °C. Then the gel was dried at 120 °C over night to form a dry gel. The dry gel was grounded and heated at 700 °C for 8 h in the flowing argon.

Measurements

Powder X-ray diffraction (XRD; Bruke D8) employing Cu Kα radiation was used to identify the crystalline phase of the material. The surface morphology was observed with a scanning electron microscope (SEM, HITACHI S-4700). The coin cell was prepared as described in Ref. [15]. The composite electrode was made from a mixture of the prepared sample, acetylene black, and polyvinylidene fluoride in a weight ratio of 80:10:10. Galvanostatic charge–discharge measurements were performed in a potential range of 3.0–4.8 V.

Results and discussion

Figure 1 shows the XRD patterns of all the $Li_3V_{2-x}Cr_x(PO_4)_3$ (x=0, 0.1, 0.25, and 0.5) samples. The patterns of the Cr-doped samples are similar to the undoped sample, and no extra reflections were observed. This indicates that Cr enters into the structure of $Li_3V_{2-x}Cr_x(PO_4)_3$ rather than forming impurities. All the samples can be indexed with a monoclinic structure with group space $P2_1/n$. The lattice parameters of the $Li_3V_{2-x}Cr_x(PO_4)_3$ (x=0, 0.1, 0.25, and 0.5) samples are calculated, and the results are listed in Table 1. As the Cr amount increases, most of the lattice parameters show a monotonous change. For $0 \le x \le 0.5$, the lattice parameters of a, b and c decrease with increasing x. But β changes ruleless with increasing x. The decrease of

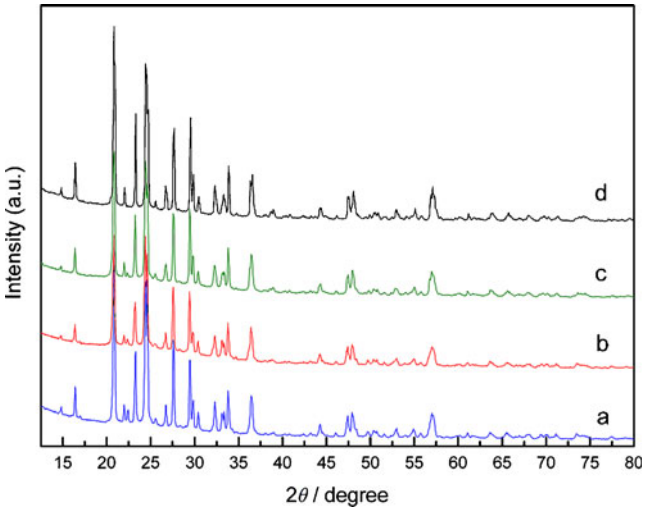

Fig. 1 The XRD patterns of the $Li_3V_{2-x}Cr_x(PO_4)_3$ samples, x=0 (**a**), 0.1(**b**), 0.25 (**c**), and 0.5 (**d**)

the lattice parameters can be attributed to the smaller radius of Cr^{3+} (0.64 Å) than that of V^{3+} (0.74 Å) or Li^+ (0.76 Å) [16–18].

The SEM images of all the samples are shown in Fig. 2. All the samples composed of agglomerated small particles. Little difference can be observed for the particle size in the SEM images, thus it is hard to correlate the electrochemical performance with the particle size.

The electrochemical characteristics of $Li_3V_{2-x}Cr_x(PO_4)_3$ (x=0, 0.1, 0.25, 0.5) are shown in Figs. 3, 4, 5, 6, and 7. Figure 3 shows the initial charge/discharge curves of the undoped and Cr-doped samples at the 0.2 C rate in the voltage range of 3.0–4.8 V. There are four plateaus in the charge curves at around 3.62, 3.69, 4.09, and 4.56, which corresponds to a sequence of phase transition processes between the single phases $Li_xV_2(PO_4)_3$ (x=3.0, 2.5, 2.0, 1.0, and 0). In charge process, the first lithium ion is extracted in two steps, 3.62 and 3.69 V, which is because of the presence of an ordered phase $Li_{2.5}V_2(PO_4)_3$. Subsequently, the second lithium ion is extracted in one single plateau of 4.09 V to form $Li_{1.0}V_2(PO_4)_3$ [19]. These initial three plateaus is related to the two lithium ions extraction which associated with the V^{3+}/V^{4+} redox couple. Finally, the third lithium ion is removed in the plateau of 4.56 V, which indicates that one switches from the V^{3+}/V^{4+} redox couple to the V^{4+}/V^{5+} redox couple. As the Cr doping amount increases, the initial two plateaus of 3.62 and 3.69 V become indistinguishable and gradually overlap to one slope. Moreover, the size of the plateau at 4.09 V obviously decreases with higher Cr doping amount. These phenomena are related to the various amount of V^{3+} in the samples. In the $Li_3V_{2-x}Cr_x(PO_4)_3$ system, the increasing of Cr^{3+} dopant (x) accompanies with the decreasing of V^{3+}

Table 1 Lattice parameters of the $Li_3V_{2-x}Cr_x(PO_4)_3$ (x=0, 0.1, 0.25, and 0.5) samples

Samples	a (Å)	b (Å)	c (Å)	β (°)
$Li_3V_2(PO_4)_3$ (x=0)	8.5481	8.5757	11.9641	90.3849
$Li_3V_{1.9}Cr_{0.1}(PO_4)_3$ (x=0.1)	8.5406	8.5742	11.9601	90.3203
$Li_3V_{1.75}Cr_{0.25}(PO_4)_3$ (x=0.25)	8.5276	8.5620	11.9486	90.1931
$Li_3V_{1.5}Cr_{0.5}(PO_4)_3$ (x=0.5)	8.5187	8.5441	11.9317	90.2597

(2-x). Because the Cr^{3+}/Cr^{4+} is inactive below 4.6 V [20], the reducing of the initial three plateaus (3.62, 3.69, and 4.09), which corresponds to the V^{3+}/V^{4+} redox couple, can be attributed to the decreasing of the active V^{3+} content in higher Cr doping amount. The capacities of the $Li_3Cr_xV_{2-x}(PO_4)_3$ (x=0, 0.1, 0.25, and 0.5) samples decrease monotonically as the x value is increased. The highest capacity is obtained for the undoped sample, which can be attributed to its largest V^{3+} amount among all the samples. Therefore, it indicates that Cr doping leads to the decreasing of the electrochemical performance for the samples in the initial cycle.

Figure 4 shows the discharge capacities of all the samples at various current densities, i. e. 0.2, 0.5, 1, and 2 C in the voltage range of 3.0–4.8 V. For each sample, the capacity monotonically decreases as the current density increases. When the same current density is applied, the capacities of the samples change as the doping amount (x) increases. At the lower current density of 0.2 C (or 0.5 C), the capacities monotonically decrease as Cr doping

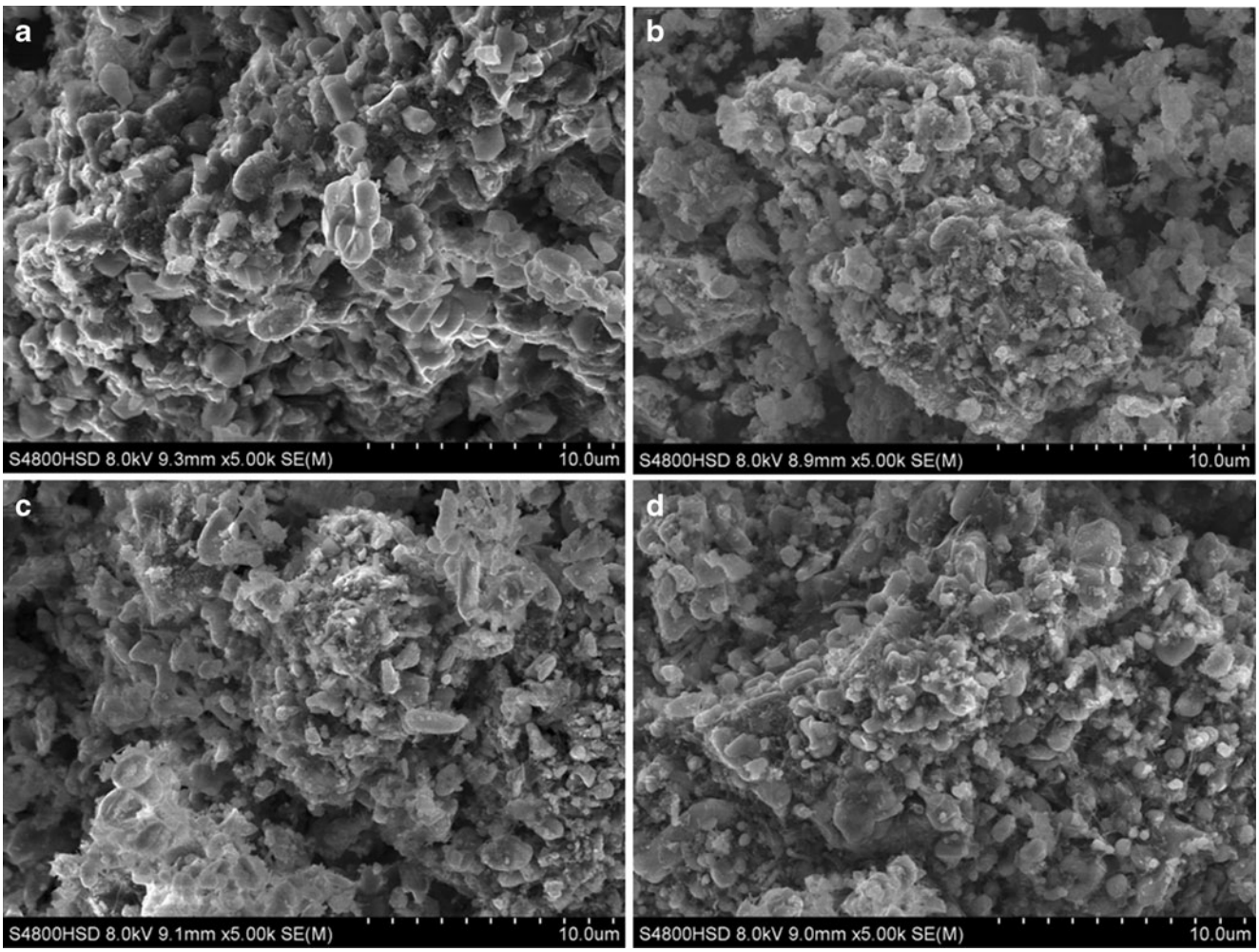

Fig. 2 The SEM images of the $Li_3V_{2-x}Cr_x(PO_4)_3$ samples, x=0 (**a**), 0.1(**b**), 0.25 (**c**), and 0.5 (**d**)

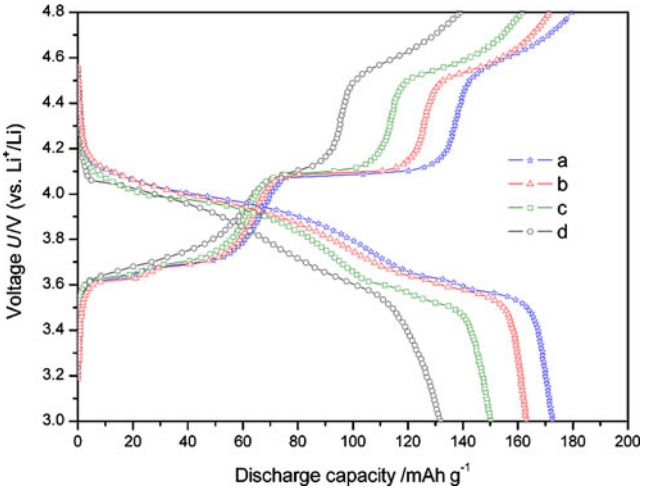

Fig. 3 The initial charge/discharge curves of the $Li_3V_{2-x}Cr_x(PO_4)_3$ samples at the 0.2 C rate in the voltage range of 3.0–4.8 V, x=0 (**a**), 0.1(**b**), 0.25 (**c**), and 0.5 (**d**)

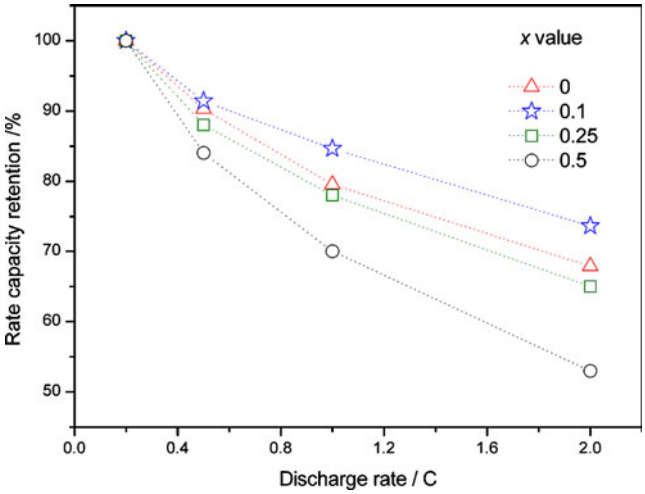

Fig. 5 The rate capacity retentions of the $Li_3V_{2-x}Cr_x(PO_4)_3$ samples at various current densities, i.e., 0.2, 0.5, 1, and 2 C in the voltage range of 3.0–4.8 V (x=0, 0.1, 0.25, and 0.5)

amount (x) increases. The highest capacity is obtained for the undoped sample. However, when the higher current density (1 or 2 C) is used, the capacity initially increases (when x is below 0.1), then turn to decreases (x>0.1) as the doping amount (x) further increases. In addition, the highest capacity is obtained for $Li_3V_{1.9}Cr_{0.1}$ $(PO_4)_3$ (x=0.1) at both current densities of 1 and 2 C.

Figure 5 shows the rate capacity retentions of all the samples at various current densities of 0.2, 0.5, 1, and 2 C in the voltage range of 3.0–4.8 V. The rate capacity retention is calculated from the ratio of the capacity at a certain current density to the capacity at the 0.2 C rate. For each sample, the rate capacity retention monotonically decreases as the current density increases. When the same current density is applied, the rate capacity retention initially increases (when x is below 0.1), then decrease as the doping amount further increases. $Li_3V_{1.9}Cr_{0.1}(PO_4)_3$ (x=0.1) shows the highest rate capacity retentions at all the current densities. Therefore, the results suggest that the Cr doping with low amount (x=0.1) improve the discharge capacity and rate capacity retention of $Li_3V_{2-x}Cr_x(PO_4)_3$ especially at high current densities.

The differential capacities (dQ/dV) of $Li_3V_{1.9}Cr_{0.1}(PO_4)_3$ (x=0.1) and undoped samples are calculated and the differential capacity versus potential (dQ/dV vs. V) curves are plotted in Fig. 6. The dQ/dV vs. V curves provide information similar to that of cyclic voltammograms. The oxidation/reduction peaks in the curve correspond to the charge/discharge plateaus in the charge/discharge curves.

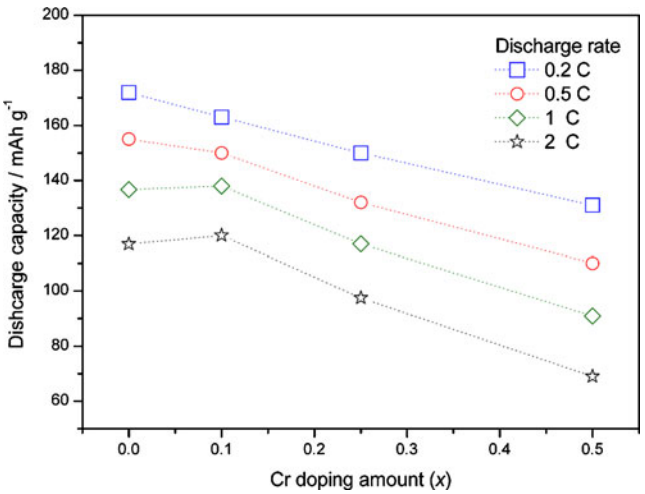

Fig. 4 The discharge capacities of the $Li_3V_{2-x}Cr_x(PO_4)_3$ samples at various current densities, i.e., 0.2, 0.5, 1, and 2 C in the voltage range of 3.0–4.8 V (x=0, 0.1, 0.25, and 0.5)

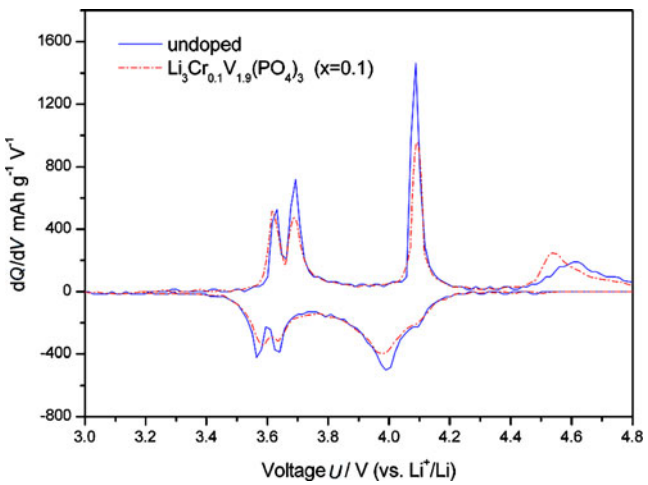

Fig. 6 The differential capacities vs. potential curves of the $Li_3V_{1.9}Cr_{0.1}(PO_4)_3$ (x=0.1) and undoped samples

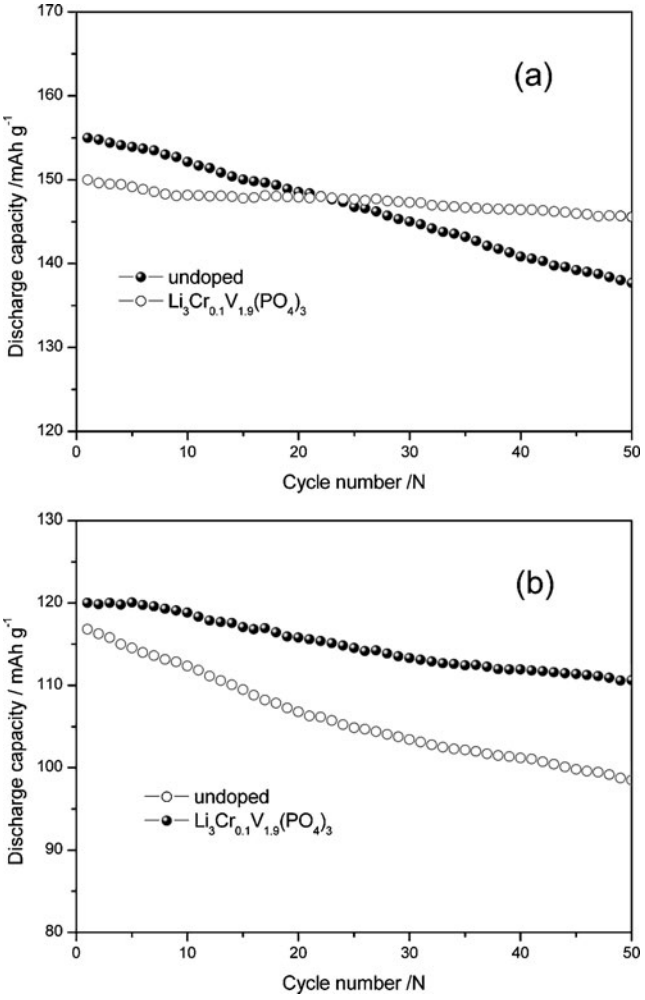

Fig. 7 The cycling performance of the $Li_3V_{1.9}Cr_{0.1}(PO_4)_3$ (x=0.1) and undoped samples (x=0) at the 0.5 C (**a**) and 2 C (**b**) rates in the voltage range of 3.0–4.8 V

As shown in Fig. 6, four oxidation peaks and three reduction peaks are observed for both samples, which is related to a sequence of transitions process between the single phase $Li_xV_2(PO_4)_3$. Compared with the undoped sample, all the redox peaks of $Li_3Cr_{0.1}V_{1.9}(PO_4)_3$ become lower and narrower. Especially, the reduction peaks at about 3.56 and 3.64 V of $Li_3V_{1.9}Cr_{0.1}(PO_4)_3$ gradually overlap to become one broad peak. The results indicate that the lithium ion insertion–deinsertion process become more disordered after Cr doping. Moreover, a shift to higher voltage of the oxidation peak at around 4.56 V is observed for $Li_3Cr_{0.1}V_{1.9}(PO_4)_3$ compared with the undoped one, which can be attributed to the changes of cation distributions and structure deformations caused by Cr doping.

Figure 7 shows the cycling performance of the $Li_3V_{1.9}Cr_{0.1}(PO_4)_3$ (x=0.1) and the undoped sample at the 0.5 and 2 C rates in the voltage range of 3.0–4.8 V. The cycling capacity retention is calculated from the ratio of the capacity after cycling to the capacity before cycling. The cycling capacity retentions of the $Li_3Cr_{0.1}V_{1.9}(PO_4)_3$ and undoped samples are 97% and 89% at the 0.5 C rate, and 92% and 84% at the 2 C rate. In both current densities, the capacity retention of the $Li_3Cr_{0.1}V_{1.9}(PO_4)_3$ is higher than that of the undoped sample, which indicates its higher cycling stability. The higher cycling stability of the $Li_3Cr_{0.1}V_{1.9}(PO_4)_3$ sample can be attributed to the effect of Cr doping. During the de/intercalation process, V^{3+} is oxidized to V^{4+} and even V^{5+}, and the crystal lattice of $Li_3V_2(PO_4)_3$ shrinks/expands. Cr^{3+} is not involved in the oxidation/reduction reaction, thus it can stabilize the crystal lattice and improve the cycling stability of $Li_3V_2(PO_4)_3$. Therefore, proper amount of Cr doping improves the stability of the structure and enhances the electrochemical performance of $Li_3V_2(PO_4)_3$.

Conclusions

$Li_3V_{2-x}Cr_x(PO_4)_3$ (x=0, 0.1, 0.25, and 0.5) are prepared by a sol–gel route. The effects of Cr doping on the structure, morphology, and electrochemical characteristics of $Li_3V_2(PO_4)_3$ are investigated. Compared with the XRD pattern of the undoped sample, the XRD patterns of the Cr-doped samples have no extra reflections, which indicates that Cr enters the structure of $Li_3V_2(PO_4)_3$. Although the capacities of the samples decrease in the initial cycle at the 0.2 C rate after Cr doping, both the rate property and cycling performance are improved with proper amount Cr doping (x=0.1). The improvement can be attributed the enhanced structure stability and the reduced particle size of $Li_3V_2(PO_4)_3$ after Cr doping, which results in the lower polarization, the higher rate property and longer cycling performance.

Acknowledgment This work is supported by the National Natural Science Foundation of China (No. 21001036, 50902041), the Basic Research Foundation of Harbin Engineering University (No. HEUFT05046), University Key Teacher by the Heilongjiang Ministry of Education (No.1155G28), Postdoctoral Foundation of Heilongjiang Province (No. LBH-Q08057), Innovation Foundation of Harbin City (No. 2009RFQXG201) and Development Program for Outstanding Young Teachers in Harbin Normal University (No. KGB200805).

References

1. Padhi AK, Nanjundaswamy KS, Goodenough JB (1997) J Electrochem Soc 144:1188–1194
2. Delacourt C, Poizot P, Tarascon JM, Masquelier C (2005) Nat Mater 4:245–260
3. Chung SY, Bloking JT, Chiang YM (2002) Nat Mater 1:123–126
4. Yin SC, Strobel PS, Grondey H, Nazar LF (2004) Chem Mater 16:1456–1465
5. Barker J, Saidi MY, Swoyer JL (2003) J Electrochem Soc 150: A684–A688

6. Huang H, Faulkner T, Barker J, Saidi MY (2009) J Power Sources 1:748–751
7. Dai CS, Chen ZY, Jin HZ, Hu XG (2010) J Power Sources 195:5775–5779
8. Quan KG, Zhao YM, An XN, Liu JM, Dong YZ, Chen L (2010) Electrochim Acta 55:1575–1581
9. Chang CX, Xiang JF, Shi XX, Han XY, Yuan LJ, Sun JT (2008) Electrochim Acta 54:623–627
10. Delacourt C, Poizot P, Levasseur S, Masquelier C (2006) Electrochem Solid State Lett 9:A352–A355
11. Rui XH, Li C, Chen CH (2009) Electrochim Acta 54:3374–3380
12. Jiang T, Pan WC, Wang J, Bie XF, Du F, Wei YJ, Wang CZ, Chen G (2010) Electrochim Acta 55:3864–3869
13. Barker J, Gover RKB, Burns P, Bryan A (2007) J Electrochem Soc 154:A307–A313
14. Ren MM, Zhou Z, Li YZ, Gao XP, Yan J (2006) J Power Sources 162:1357–1362
15. Zhang S (2007) Electrochim Acta 52:7337–7342
16. Chen Y, Zhao Y, An X, Liu J, Dong Y, Chen L (2009) Electrochim Acta 54:5844–5850
17. Yang MR, Ke WH (2008) J Electrochem Soc 155:A729–A732
18. Ou X, Liang G, Wang L, Xu S, Zhao X (2008) J Power Sources 184:543–547
19. Yin SC, Grondey H, Strobel P, Anne M, Nazar LF (2003) J Am Chem Soc 125:10402–10411
20. Morgan D, Ceder G, Saidi MY, Barker J, Swoyer J, Huang H, Adamson G (2002) Chem Mater 14:4684–4693